

# Quantum chaos dynamics in long-range power law interaction systems

Xiao Chen<sup>1</sup> and Tianci Zhou<sup>2,1</sup>

<sup>1</sup>*Kavli Institute for Theoretical Physics,  
University of California, Santa Barbara, CA 93106, USA*

<sup>2</sup>*University of Illinois, Department of Physics,  
1110 W. Green St. Urbana, IL 61801 USA*

(Dated: May 9, 2022)

## Abstract

We use out-of-time-order correlator (OTOC) to diagnose the propagation of chaos in one dimensional long-range power law interaction system. We consider a model called Brownian quantum circuit, which allows us to derive the master equation governing the operator dynamics and therefore transforms the evolution of OTOC to a classical stochastic dynamics problem. We find that the chaos propagation relies on two parameters: the number of qubits  $N$  on each site (the onsite Hilbert space dimension) and the power law exponent  $\alpha$ . We use OTOC to define light cone and find that in the small  $N$  limit ( $N = 1$ ), there are three light cone regimes as we vary  $\alpha$ : (1) a log light cone regime when  $1 < \alpha < 2$ , (2) a sublinear power law light cone regime when  $2 < \alpha < 4$  and (3) a linear light cone regime when  $\alpha > 4$ . We further study the scaling behaviors of OTOC in the vicinity of light cone. When  $\alpha$  slightly exceeds 4, the OTOC has essentially the same diffusive broadening as systems with short-range interactions, suggesting that the locality is fully recovered even if the interaction is non-local. According to the different scaling behavior of OTOC, we divide the power law regime into two subregimes. For the subregime with smaller  $\alpha$ , OTOC takes a simple scaling form  $(t^b/x)^c$ , which eventually crosses over to  $\exp(\lambda t)/x^c$  as we move deep into the log light cone regime by reducing  $\alpha$ . We also study the operator growth in the large  $N$  limit and find it to be remarkably different. At large but finite  $\alpha$ , although we can observe linear light cone regime, there is always a transition to log light cone at late time, implying the locality is never fully recovered as long as  $\alpha$  is finite. Our result provides a unified physical picture for chaos dynamics in long-range power law interaction system and can be generalized to higher spatial dimensions.

## I. INTRODUCTION

Quantum many-body chaos has been a subject of continuous interest in the past years and has drawn a lot of attention from various subfields of physics. The dynamics of chaos can be diagnosed by out-of-time-order correlator (OTOC)<sup>1</sup>,

$$C(t) = -\langle [\hat{O}_1(t), \hat{O}_2]^2 \rangle_\beta \quad (1.1)$$

which measures the non-commutativity between a Heisenberg operator  $\hat{O}_1(t) = e^{i\hat{H}t}\hat{O}_1e^{-i\hat{H}t}$  and a time independent simple operator  $\hat{O}_2$ . It has been shown in some systems with all-to-all interactions, OTOC can grow exponentially in time, i.e,  $C(t) \sim \exp(\lambda t)$ , where  $\lambda$  is a quantum analogy of Lyapunov exponent<sup>2-6</sup>. These systems in the literature are referred to as “fast scramblers”<sup>3</sup>.

On the other hand, in system with short-ranged interaction,  $C(t, x)$  for two operators  $\hat{O}_1(t)$  and  $\hat{O}_2(x)$  separated by distance  $x$  is equal to zero at early time and starts to grow at time  $t \approx x/v_B$ . Here  $v_B$  is the so-called butterfly velocity<sup>7,8</sup>, which characterizes the ballistic propagation of chaos and is constrained by the Lieb-Robinson bound<sup>9</sup>. In general, the explicit form of OTOC is complicated and is model dependent. However, it has been shown that there could be universal scaling forms in some special cases. For instance, in the local random circuit model,  $C(x, t) \sim \exp(-a(x - v_B t)^2/t)$  in the vicinity of  $x - v_B t = 0$ <sup>10,11</sup>. This diffusive wavefront picture has been shown to work successfully in chaotic spin systems with small onsite Hilbert space. On the other hand, in some chaotic systems with large onsite Hilbert space,  $C(x, t)$  can form a stable traveling wave  $\sim \exp(\lambda(t - x/v_B))$  when  $x \approx v_B t$ <sup>7</sup>. Recently, other possible scaling forms have been proposed which also follow the Lieb-Robinson bound<sup>12,13</sup>.

However, the above physics needs to be modified if we consider a system with long-range power law interaction  $1/r^\alpha$ . In these systems, Hastings and Koma show that the spreading of quantum information is bounded by a logarithmic light cone if  $\alpha > D$  where  $D$  is the spatial dimension<sup>14</sup>. This bound is subsequently improved in Ref. 15, where the authors show that if  $\alpha > 2D$ , a local perturbation can spread out algebraically in time rather than exponentially, indicating the existence of a power law light cone. All these bounds suggest that the chaos propagation in power law interaction system could be much faster than system

with short-range interaction.

Keeping the above physical picture in mind, we study chaos dynamics in system with power law interaction and in particular we try to answer two questions: (1) how fast is the propagation of chaos in power law interaction systems and (2) what are the possible scaling forms of OTOC. To answer these two questions, we study a toy model called Brownian quantum circuit model, whose unitary evolution operator performs a Brownian motion in the space of allowed interactions<sup>16–18</sup>. We will focus on the one dimensional system in which there are  $N$  qubits at each site. We will demonstrate the emergent light cone from the perspective of chaos propagation and discuss the appearance of *linear*, *power law* and *logarithmic* light cones, which are consistent with bounds proposed in Ref. 15. The structure of the light cone is determined by two important parameters: the dimension of onsite Hilbert space set by  $N$  and the power law interaction exponent  $\alpha$ . At large  $\alpha$ , we observe a linear light cone regime, which usually occurs in systems with local interaction. In these systems, the chaos propagation speed can be quantified by the butterfly velocity  $v_B$  which is the slope of the light cone<sup>7,8</sup>. This concept can be generalized to power law or logarithmic light cone regimes in which  $v_B$  grows algebraically or exponentially in time. Once we have a clear understanding of the light cone and  $v_B$ , we can further investigate the scaling forms of OTOC. We summarize the main results in Fig. 1.

One advantage of using Brownian quantum circuit is that we can derive the master equation governing the operator dynamics. Although we cannot directly solve the master equation (unless in the limits  $\alpha = 0, \infty$ ), we can perform numerical simulation on classical stochastic dynamics determined by the master equation and obtain  $C(x, t)$ . This method allows us to compute lattice models with *thousands* of sites which greatly reduces the finite size effect. Notice that if we directly simulate quantum spin systems with small system size, the finite size effect could be very strong, especially in the non-local power law interaction systems<sup>19</sup>.

The rest of the paper is organized as follows. In Sec. II, we discuss Brownian quantum circuit and derive the master equation governing the operator growth in systems with power law interactions. In Sec. III, we perform numerical simulation on  $N = 1$  case and the appearance of various light cone structure as we tune  $\alpha$ . We then perform data collapse on  $C(x, t)$  and discuss possible scaling functions of OTOC in Sec. III B. In Sec. IV, we numerically solve the master equation in the large  $N$  limit. We discuss the emergent light

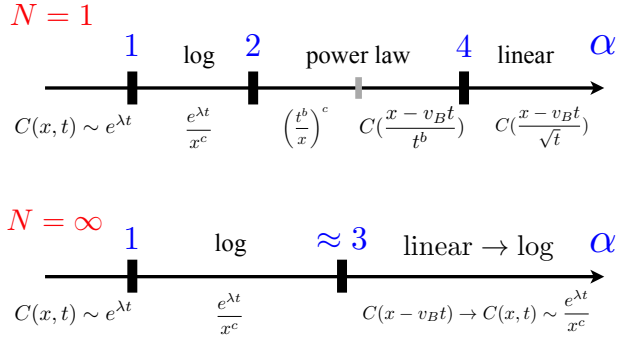


FIG. 1. Upper panel: The light cone behavior and scaling form of OTOC as a function of  $\alpha$  at  $N = 1$ . Notice that the power law regime can be further divided into two subregimes according to the scaling form of OTOC. Lower panel: The light cone structure and scaling form of OTOC as a function of  $\alpha$  in the large  $N$  limit.

cone and scaling functions of OTOC and compare the results with small  $N$  limit. Finally, we summarize our results and discuss possible future directions in Sec. V.

## II. THE BROWNIAN QUANTUM CIRCUIT AND MASTER EQUATION

We begin by introducing the dynamics in operator space. Let  $B_\mu$  be a complete orthonormal operator basis, any operator can be expanded as

$$O(t) = \sum_{\mu} \alpha_{\mu}(t) B_{\mu}. \quad (2.1)$$

Under *unitary* time evolution,  $|\alpha_{\mu}(t)|^2$  can be interpreted as the probability of the basis  $B_{\mu}$ , where the total probability for properly normalized operator  $\sum_{\mu} |\alpha_{\mu}(t)|^2 = 1$  is conserved.

In a generic chaotic system, the operator dynamics is complicated and it is usually hard to see how  $|\alpha_{\mu}(t)|^2$  evolves. However, recent study of random unitary circuits suggests that in the chaotic systems with local interaction, the spreading of an initially local operator can be mapped to a classical crystal growth process and the coarse-grained dynamics exhibits universal behavior in the operator space<sup>10,11</sup>. This physical picture is later confirmed and generalized in other examples of one dimensional chaotic spin chain models<sup>12,20</sup>. Inspired by these findings, we take one dimensional models with non-local power law interaction and explore whether a similar mechanism exists in operator space.

The model we consider has  $L$  sites, each of which is a quantum dot and has  $N$  spin- $\frac{1}{2}$

degrees of freedom. The model contains only the couplings between spins from different sites (dots). To be concrete, let  $\sigma^\mu(i, n)$  be the Pauli sigma matrix of  $n$ th spin at dot  $i$ , and the Hamiltonian is

$$H = \sum_{i \neq j} \sum_{n, m=1}^N \sum_{\mu, \nu=0}^3 J_{\mu\nu}(i, j, m, n, t) \sigma^\mu(i, m) \sigma^\nu(j, n). \quad (2.2)$$

where the coupling constant  $J$  is proportional to a power function of the distance  $\frac{1}{|i-j|^\alpha}$ . In order to make the model tractable, we take the coupling to be the Brownian motion. Dividing the evolution into short periods of  $\Delta t$  intervals, the coupling at the  $s$ -th interval is approximately

$$J_{\mu\nu}(i, j, m, n, t = s\Delta t) = \Delta B_{i,j,m,n}^s(t) \frac{g}{|i-j|^\alpha}, \quad g = \sqrt{\frac{1}{8}} \quad (2.3)$$

where  $\Delta B_{i,j,m,n}^s(t)$  are independent Gaussian random numbers with variance proportional to  $\Delta t$ . The complete time evolution is generated in the continuum limit of

$$e^{-iH_s \Delta t} e^{-iH_{s-1} \Delta t} \dots \quad (2.4)$$

This type of models is called the Brownian quantum circuit. The time evolution is a random walk on the unitary group in the direction of allowed couplings. The statistical average of the operator spreading is analytically tractable and many of the variants<sup>12,17,21,22</sup> have been used to study the dynamics of quantum chaos.

In the one dimensional model we consider, the operator dynamics is fully determined by the operator height distribution function  $f(\mathbf{h})$ , i.e.,

$$f(\mathbf{h}, t) = \sum_{\text{height}(B_\mu)=\mathbf{h}} |\alpha_\mu(t)|^2 \quad (2.5)$$

where height  $\mathbf{h}$  is a  $L$ -component vector. The height of a Pauli basis  $B_\mu$  on each site is the number of non-identity operators therein. The distribution groups all the probability contributions whose corresponding basis has height  $\mathbf{h}$ . The height distribution is important since it contains all the necessary information of operator growth and the mean height is equal to OTOC<sup>12,17,23</sup>. In our previous paper<sup>17</sup>, we studied a Brownian quantum dot of  $N$

qubits with all-to-all interaction and we derived the master equation of  $f(h)$  with  $h \in [0, N]$  as the height on a single dot. Following a similar method, we can show that the evolution of the joint distribution  $f(\mathbf{h})$  in a one dimensional model is governed by the master equation

$$\begin{aligned} \frac{\partial f(\mathbf{h}, t)}{\partial t} = & \sum_{j \neq i} 3D_{ij} h_{i+j} f(\mathbf{h} - \mathbf{e}_i, t) + \sum_{j \neq i} D_{ij} h_{i+j} f(\mathbf{h} + \mathbf{e}_i, t) \\ & - \left\{ \sum_{j \neq i} 3D_{ij} h_{i+j} (N - h_i) + \sum_{j \neq i} D_{ij} h_{i+j} h_i \right\} f(\mathbf{h}, t) \end{aligned} \quad (2.6)$$

where the coefficient  $D_{ij}$  is  $\frac{1}{|i-j|^\alpha}$ . If we take  $D_{ij}$  to be short-range interaction, the above equation is similar to the one derived in Ref. 12. Once we know  $f(\mathbf{h})$ , we can compute the average height  $\bar{h}_j$  at each site and obtain the spatial and temporal profile of OTOC. For instance, if we take  $\hat{O}_1(t=0)$  as a simple operator at dot  $i$  and  $\hat{O}_2$  at dot  $j$ , the average height  $\bar{h}_j$  is equal to OTOC  $C(x = |j - i|, t)$  defined in Eq. (1.1).

We first deal with the case of  $N = 1$ , representing spin chain with small onsite Hilbert space dimensions. The height at each dot can only take 0 or 1 and therefore the model is a nonequilibrium kinetic Ising model<sup>24</sup>. The master equation becomes,

$$\begin{aligned} \frac{\partial f(\mathbf{h}, t)}{\partial t} = & \sum_{j \neq i} 3D_{ij} h_{i+j} f(\mathbf{h} - \mathbf{e}_i, t) + \sum_{j \neq i} D_{ij} h_{i+j} f(\mathbf{h} + \mathbf{e}_i, t) \\ & - \{3D_{ij} h_{i+j} (1 - h_i) + D_{ij} h_{i+j} h_i\} f(\mathbf{h}, t) \end{aligned} \quad (2.7)$$

This equation describes the Markov process shown in Fig. 2. The interaction induces a transition rate of height change: the dot  $j$  with height  $h_j = 1$  will increase the height  $h_i$  from 0 to 1 with rate  $3D_{ij}$  while decrease its height from 1 to 0 with rate  $D_{ij}$ . The spin here on each site has Hilbert space dimension 2. This can be directly generalized to a  $q$  dimensional  $\mathbb{Z}_q$  rotor and we expect the rate becomes  $4(1 - \frac{1}{q^2})D_{ij}$  and  $\frac{4}{q^2}D_{ij}$ . In the  $q \rightarrow \infty$  limit, the rate of flipping down is zero.

The master equation in Eq.(2.7) has two simple limits that have been studied by previous literatures.

When  $\alpha = 0$ , the interaction is equally weighted between any pair of quantum dots. Therefore we can view this as an effective single quantum dot with  $L$  spins. Because all dots are identical, the full distribution only depends on the total height  $\sum_i h_i$  (which is the height of the effective single dot). The OTOC has an initial exponential growth and can be

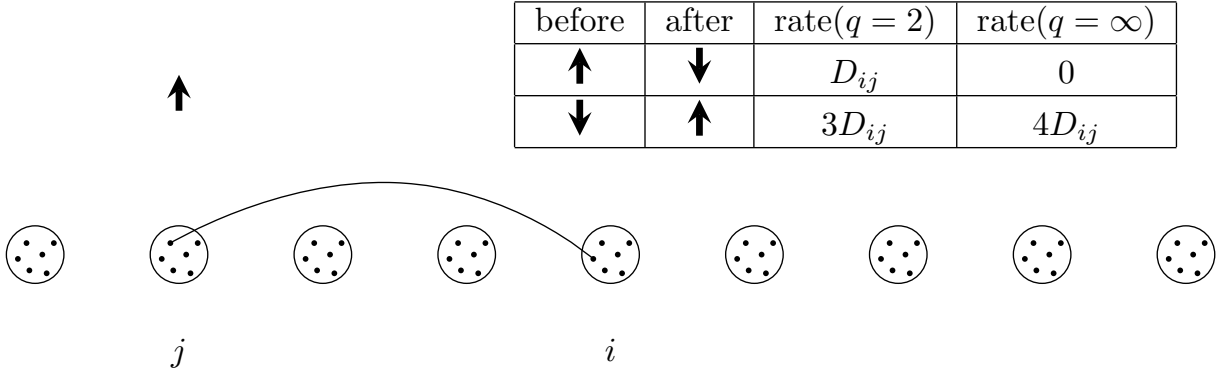


FIG. 2. Transition rate induced by an interaction term between spins from dot  $j$  and dot  $i$ . The flipping rate of  $N = 1$  case (shown in the table) for spin at  $i$  is only nonzero when spin  $j$  is up; the rate for flipping up is higher, giving rise to operator spreading.

described by a general logistic function behavior over the entire time<sup>17</sup>. The same scaling behavior should hold even when  $\alpha$  is close to 0 that the locality is completely lost.

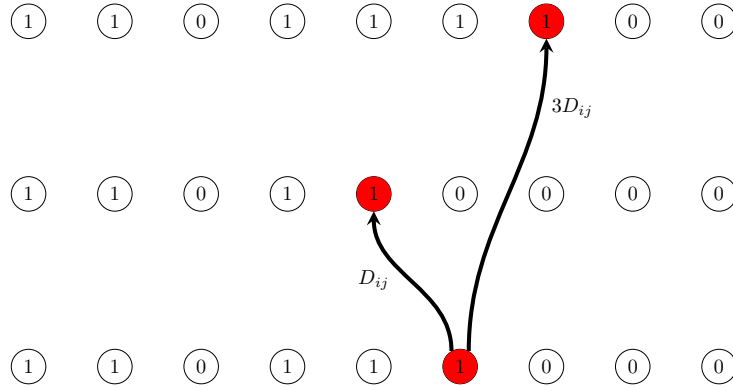


FIG. 3. End point of an operator. The figure shows typical height configurations when  $\alpha = \infty$ . The red dot is defined to be the right most dot with height 1. The dynamics of the height in thermodynamic limit only occurs at nearest neighbor site. The arrow labels the transition rate from the bottom state to the upper ones. There are also flipping processes to the left of the end point, but it quickly equilibrates.

When  $\alpha = \infty$ , the transition rate is restricted to the nearest neighbor dots, *i.e.*  $D_{ij} \neq 0$  only when  $i = j \pm 1$ . We set the initial condition to be  $h_1 = 1$  with rest of  $h_j = 0$ . As shown in Fig. 3, a typical height configuration in this limit will have a regime with high density of  $h = 1$  on the left and a  $h = 0$  domain on the right. The red dot is the right most one with height 1, which we will call the end point. In the  $q \rightarrow \infty$  limit, one can view this as a domain wall between  $h = 1$  domain and  $h = 0$  domain. This point performs a biased random walk towards the right and the mean value  $\overline{h(x, t)}$  propagates ballistically with the

front broadening diffusively. This wave front interpolates  $h = 0$  domain and the left side of the end point, which quickly equilibrates to have an average value of  $h_{\text{sat}} = \frac{3}{4}$ . This gives the same picture described by the random local unitary circuit<sup>10,11</sup>. However, as we will show later, this biased random walk picture breaks down as we reduce  $\alpha$  for two reasons: The end point can have non-local random walks that is not restricted to neighbors within fixed radius. The regime on the left of the end point does not immediately equilibrate after the front sweeps through. Hence the end point distribution, though can be defined, does not directly relate to the mean height or OTOC. We need to directly compute the mean height by using the master equation.

The full joint distribution  $f(\mathbf{h})$  governed by Eq.(2.7) or Eq.(2.6), resembles a many-body wave function of the tensor product of heights. Recently, Ref. 12 used the matrix product state (MPS) based approaches to represent and evolve  $f(\mathbf{h}, t)$  in Brownian circuit with local interaction and studied the crossover from large  $N$  to small  $N$  limit. We here directly simulate the Markov process that generate and sample  $f(\mathbf{h})$  in  $N = 1$  case. We will use this method to analyze the resulting light cone structure, butterfly velocities and the scaling form of OTOC in Sec. III.

In the end, we briefly mention the  $N \rightarrow \infty$  limit. In this case, we study the normalized height  $\underline{h} = \frac{h}{N}$ , which can continuously vary from 0 to 1 in the  $N \rightarrow \infty$  limit. The height fluctuation in the Markov process is an order  $\mathcal{O}(\frac{1}{N})$  effect – we are now in the mean field limit. Taking both the rates of increasing and decreasing the height into account, we can write down the evolution equation for  $\underline{h}(x, t)$ ,

$$\begin{aligned} \frac{\partial \underline{h}(x, t)}{\partial t} &= \int dy \underline{h}(y, t) D(y, x) (1 - \underline{h}(x, t)) - \frac{1}{3} \int dy \underline{h}(y, t) D(y, x) \underline{h}(x, t) \\ &= \int dy \underline{h}(y, t) D(y, x) \left(1 - \frac{1}{h_{\text{sat}}} \underline{h}(x, t)\right) \end{aligned} \quad (2.8)$$

where the kernel  $D(x, y)$  is  $\frac{1}{|x-y|^\alpha}$ . Solving this equation gives the light cone and the full history of height (OTOC). We can take the same initial condition, but since the growth on the single dot is not of interest here, we simply set  $\underline{h}(x = 1, t = 0) = 1$  instead. The full analysis of this equation will be performed in Sec. IV.

Here we briefly discuss the two simple limits at  $\alpha = 0, \infty$ . When  $\alpha = 0$ , the result should match an effective quantum dot with  $NL$  spins. In the  $\alpha \rightarrow \infty$  limit,  $D_{ij}$  takes nonzero value only when  $i = j \pm 1$ . Therefore the evolution equation for  $\underline{h}(x, t)$  can be written in

the following form

$$\partial_t \underline{h}(x, t) = D(2\underline{h}(x, t) + \partial_x^2 \underline{h}(x, t))(1 - \frac{1}{h_{\text{sat}}} \underline{h}(x, t)) \quad (2.9)$$

This equation is very similar to the Fisher-Kolmogorov-Petrovsky-Piskunov (FKPP) equation<sup>25,26</sup>, which has a stable traveling wave solution<sup>12,27,28</sup>. In contrast, the  $N = 1$  solution has a ballistic wave solution with diffusive wavefront.

### III. NUMERICAL SIMULATION AT $N = 1$

#### A. The formation of light cone

We numerically simulate the Markov process with initial condition

$$h(x = 1, t = 0) = 1, \quad h(x > 1, t = 0) = 0 \quad (3.1)$$

and open boundary condition. In each run of the simulation (one sample),  $h(x, t)$  at fixed time  $t$  is a classical configuration with 0 or 1 on each site. We take  $L$  to have order  $10^3$  and take average over 20000 samples to obtain  $\overline{h(x, t)}$ . Under this circumstance,  $\overline{h(x, t)}$  can be treated as a continuous function of  $x$  and  $t$ . We take  $L = 1000$  and  $L = 2000$  to estimate the finite size effect.

After sufficiently long time evolution,  $\overline{h(x, t)}$  will approach the steady state value  $\overline{h(x, t \rightarrow \infty)} = h_{\text{sat}} = 0.75$ . In contrast to common interest of Markov process, our focus here is not the steady state, but the entire relaxation dynamics towards it. In particular, we will focus on the propagation of chaos and the formation of the effective light cone.

As the first step, we compute  $\overline{h(x, t)}$  at  $\alpha = 0$  as a benchmark. In this limit, the transition probability set by  $D_{ij}$  is independent of the locations of two spins and  $\overline{h}$  quickly becomes uniform on each site. As we mentioned earlier, the total height is the height in the effective single quantum dot<sup>17</sup>. Indeed the result matches if we rescale  $D_{ij}$  by  $L$ .

We now turn to the numerical simulation for  $\alpha > 0$ . The physics of  $\alpha < 1$  is similar to the case of  $\alpha = 0$ . The quantum information spreads out almost instantaneously to the entire system and therefore  $\overline{h(x, t)}$  is independent of  $x$ . This can be clearly observed in Fig. 4(a).  $\overline{h(t)}$  has an exponential growth in early time with decreasing Lyapunov exponent

$\lambda$  for increasing  $\alpha$ .

The light cone emerges when  $\alpha > 1$ . We define the light cone to be the boundary  $t_{LC}(x)$ , below which  $\overline{h(x,t)}$  is smaller than the threshold value. In our simulation, we set this threshold to be  $h_{\text{sat}}/2 = 0.375$ . As shown in Fig. 4(b), when  $\alpha = 1.5$ , we observe that the boundary curve is a logarithmic function of  $x$ , indicating that the butterfly velocity  $v_B \equiv x/t_{LC}$  grows exponentially in time. The coefficient of the logarithmic curve is increasing for increasing  $\alpha$ .

When  $\alpha > 2$ , we find a power law light cone  $t_{LC} \sim x^\xi$  with  $\xi < 1$ (Fig. 4(c)). As we increase  $\alpha$ , this power law light cone is becoming increasingly linear (Fig. 5(b)). Numerically, we find the linear light cone emerges as  $\alpha$  exceeds 4, which usually occurs in systems with finite range of interactions. The power law or linear light cone in the range  $\alpha > 2$  satisfies the light cone bound proposed in Ref. 15.

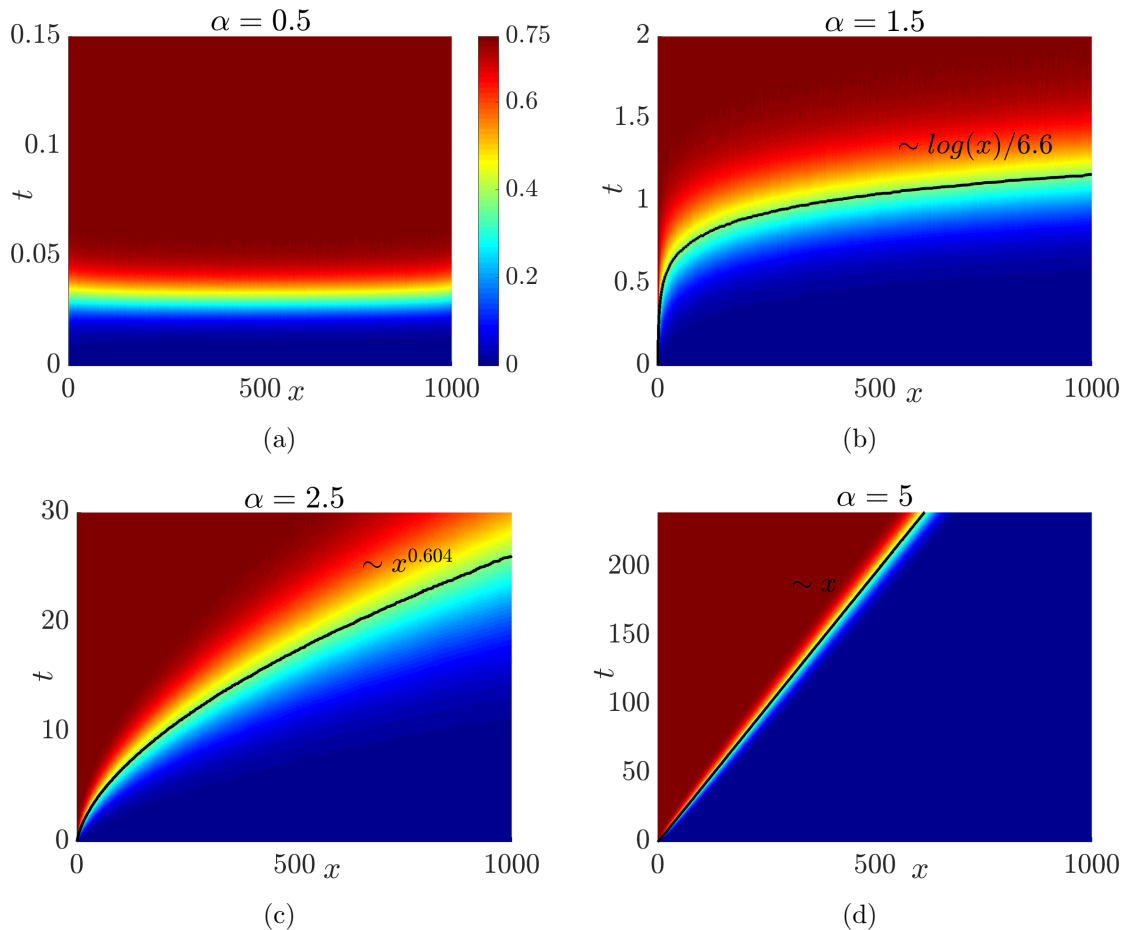


FIG. 4. The spreading of OTOC at various exponent  $\alpha$ . On the black line in (b) (c) and (d), OTOC takes value  $\overline{h} = h_{\text{sat}}/2$ .

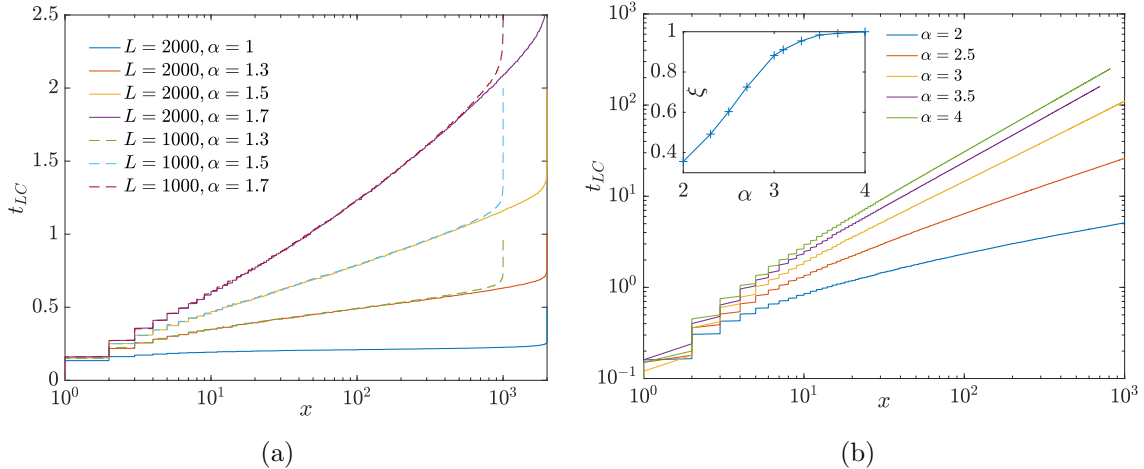


FIG. 5. (a) The curves are plotted on the semi-log scale to show the log light cone behavior when  $\alpha < 2$ . The solid lines are for  $L = 2000$ , while the dashed lines are for  $L = 1000$ . The logarithmical scaling behavior does not change as we vary system size. (b) The power law light cone  $t = x^\xi$  is shown on the log-log scale when  $\alpha > 2$ . In the inset, we extract the exponent  $\xi$  at various  $\alpha$ .

## B. The scaling form of OTOC

To better understand the propagation of local perturbation to the entire of system, we present the spatial profile  $\overline{h(x)}$  at different times for various  $\alpha$  in the insets of Fig. 6. The front of the  $\overline{h(x)}$  profile is the regime which interpolates the regimes of  $h = \frac{3}{4}$  and  $h = 0$ . We define the butterfly velocity  $v_B$  such that at  $\overline{h(v_B t, t)} = \frac{1}{2} h_{sat}$ . As we can see in Fig. 6, the front broadens in time. We give a qualitative description by data collapsing:

$$h(x, t) \rightarrow h\left(\frac{x - v_B t}{f(t)}\right) \quad (3.2)$$

where we first navigate to the vicinity of the wave front and then probe the possible broadening by the choice of the function  $f(t)$ .

As shown in Fig. 6(a), the mean height for  $\alpha = 5$  fits well with the scaling argument  $(x - v_B t)/\sqrt{t}$ . The front of  $\overline{h(x)}$  broadens diffusively as it propagates to the right with a constant butterfly velocity  $v_B$ . Here  $v_B$  can also be determined from the end point distribution  $\rho(x)$ , which is a Gaussian distribution moving to the right with  $v_B$  and broadens diffusively (see Fig. 7(a)). In Fig. 6(a), we check that the mean height  $\overline{h(x)}$  is equal to the front area of  $\rho(y)$ , i.e, a complementary error function by  $h_{sat} \int_x^\infty \rho(y) dy$ . We notice similar behaviors for other values of  $\alpha > 4$  with  $v_B$  decreasing for increasing  $\alpha$ . These results provide strong

evidence that the physics at  $\alpha > 4$  is essentially the same as the Brownian circuit with local interaction discussed in Sec. II.

As we reduce  $\alpha$  to 4, the scaling collapse suggests that the front of  $\overline{h(x,t)}$  still broadens as  $1/\sqrt{t}$  (Fig. 6(b)). However, the right side of  $\rho(x)$  is no longer a Gaussian tail due to the non-local random walk of the end point. As a consequence,  $\overline{h}$  after collapsing is not strictly the complementary error function but closer to an exponential decay function on the right side. This mechanism is discussed in our previous work<sup>29</sup> that leads to the temporal near-exponential growth of  $\overline{h(t)}$  (see Fig. 8(a)).

Further reducing  $\alpha$ , we enter into the power law light cone regime  $t_{LC}(x) = x^\xi$  with  $\xi < 1$ . The locality is gradually lost. For  $2.5 \leq \alpha \leq 3.5$ , we empirically take the scaling parameter as  $(x - v_B(t)t)/t^b$  with  $b > 0.5$ . The front still broadens with scaling  $t^b$  and  $b$  increases when we decrease  $\alpha$  (Fig. 6(c) and Fig. 6(d)). The right side of  $\rho(x)$  also has a long tail (Fig. 7(c)). But now  $\overline{h(x)} \neq h_{\text{sat}} \int_x^\infty \rho(y)dy$ , and  $\rho(x)$  is not as informative. When  $2 < \alpha < 2.5$ , the lightcone becomes so wide that a good scaling argument is  $\frac{x}{t^b}$  with  $b \approx \frac{1}{\xi}$ . In Fig. 8(b), we provide numerical evidence that  $\overline{h(t)}$  for fixed  $x$  is a power-law function of  $t$  before it saturates to a constant. This means in this regime,

$$\overline{h(x,t)} \sim (t^b/x)^c \quad (3.3)$$

when it is much smaller than the saturation value.

Finally we reach log light cone regime when  $\alpha < 2$ . We again choose the scaling parameter  $x/(v_B(t)t)$  to collapse all the curves into a single curve. Notice that in this regime  $v_B$  is exponentially growing with  $t$  (Fig. 6(f)). Deep inside the log light cone regime, we find that  $\overline{h(x,t)}$  approaches a simple scaling form  $\exp(\lambda t)/x^c$  as long as  $\overline{h(x,t)} \ll 1$ . The above data collapse results imply the existence of the universal scalings in the long-range power law interaction at small  $N$  limit.

#### IV. LARGE $N$ LIMIT

In the large  $N$  limit, we solve Eq. (2.8) to obtain  $\underline{h}(x,t)$ . The normalized height is the same as the average height, so we will call it  $\overline{h(x,t)}$  in this section.

We first study the light cone structure as we vary  $\alpha$ . By using the same method discussed

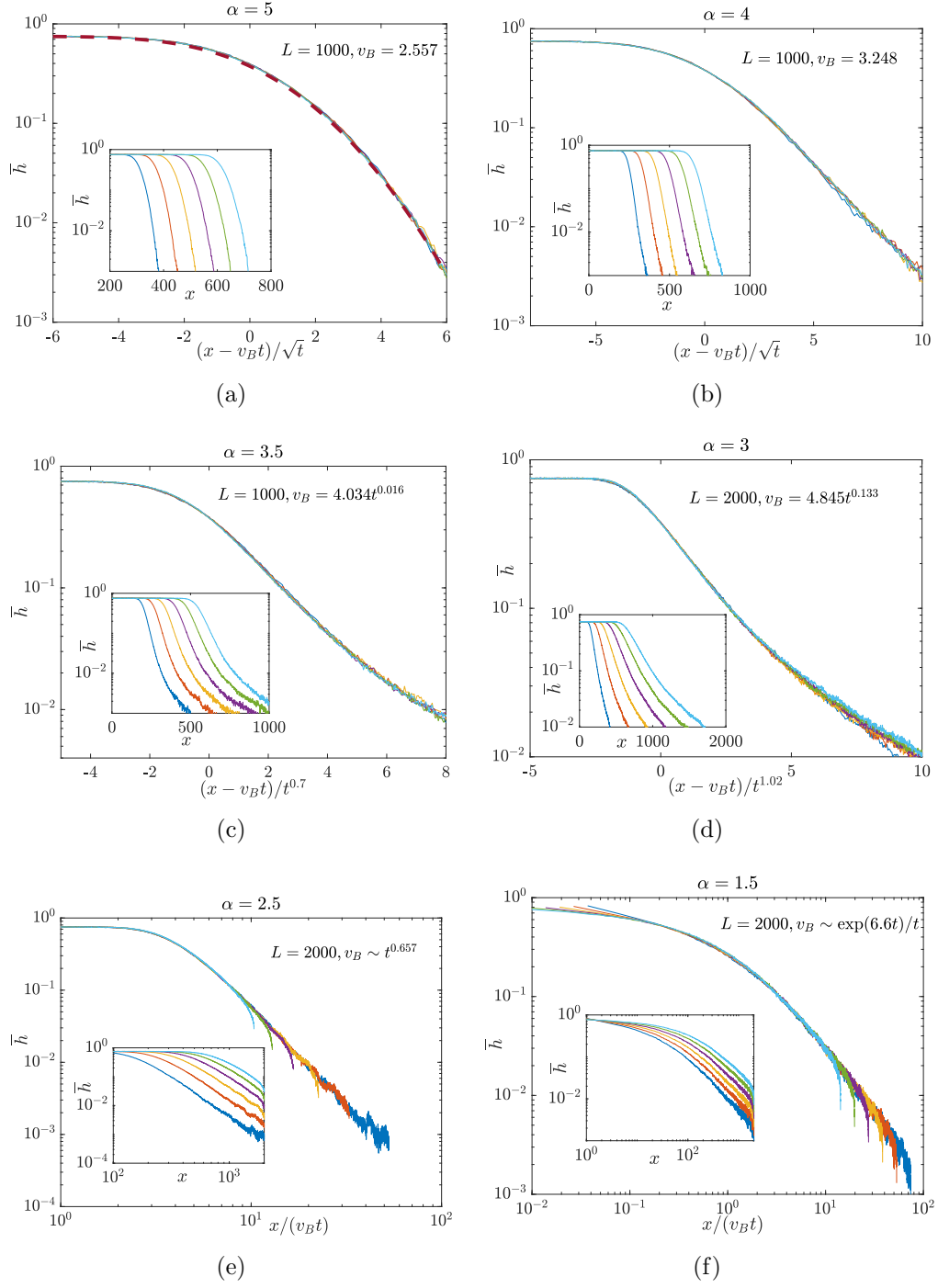


FIG. 6. Data collapse of  $\overline{h(x)}$  curves at various  $t$  on the semilog scale. The curves before collapsing are shown in the inset. The parameters  $v_B$ ,  $v$  and  $\xi$  are obtained by fitting the light cone in Fig. 4 and Fig. 5. (a) The curves in the inset have  $t \in [120, 240]$  in steps 24. The dashed line is the complementary error function  $\frac{3}{8}\text{erfc}(x/3.2)$ . (b) The curves in the inset have  $t \in [75, 200]$  in steps 25. (c) The curves in the inset have  $t \in [48, 128]$  in steps 16. (d) The curves in the inset have  $t \in [24, 84]$  in steps 12. (e) The curves in the inset have  $t \in [9, 24]$  in steps 3. (f) The curves in the inset have  $t \in [0.5, 0.75]$  in steps 0.05. The deviations at large  $x/(v_B t)$  is due to finite size effect.

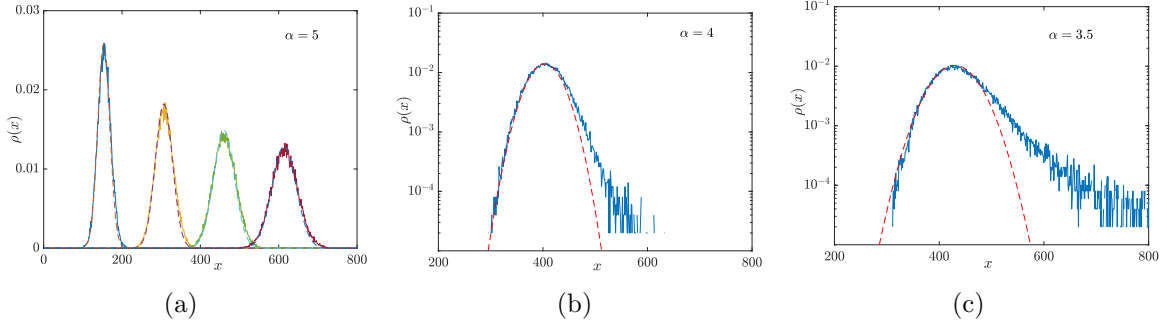


FIG. 7. (a) The solid curves are the end point distribution  $\rho(x)$  at various  $t$  when  $\alpha = 5$ . The dashed curves are the Gaussian packets which broaden diffusively with the time. (b) The solid curve is  $\rho(x)$  at  $\alpha = 4$  on the semilog scale. The dashed curve is the Gaussian packet. We can clearly see there are some deviations at the wavefront. (c) The same as (b) with  $\alpha = 3.5$ .

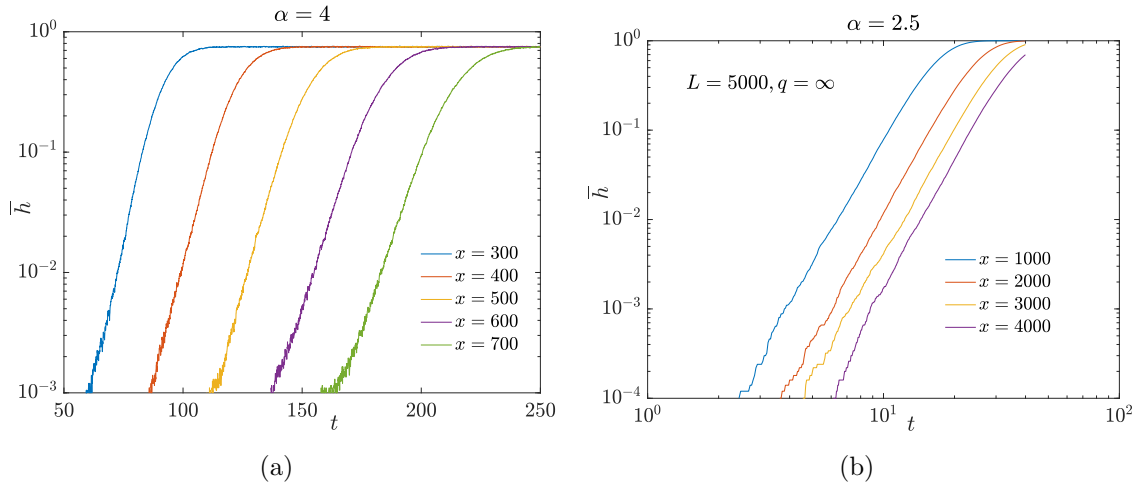


FIG. 8. (a) The temporal growth of  $\overline{h(t)}$  at different  $x$  on the semi-log scale at  $\alpha = 4$ . The straight line behavior suggests that  $\overline{h(t)}$  grows exponentially in time before it saturates to  $3/4$ , (b) The temporal power law growth of  $\overline{h(t)}$  at different  $x$  on the log-log scale at  $\alpha = 2.5$ . Notice that to obtain a clear power law behavior, we work on system with larger system size  $L = 5000$ . To simplify the numerical simulation, we take  $q = \infty$ , in which the transition probably from  $h = 1 \rightarrow h = 0$  is always zero. The physics is the same as  $q = 2$  case.

in the previous section, we notice that at large  $\alpha$ , there is a transition from linear light cone to log light cone at a critical distance  $x_c$  (see Fig. 9(a)). This structure is further presented in Fig. 9(b), where we find three interesting phenomena as we tune  $\alpha$ :

1. The log light cone scales as  $t_{LC} \sim \alpha \log x$ .
2. The butterfly velocity in the linear light cone regime is independent of  $\alpha$ .
3. The transition from linear light cone to log light cone occurs at the intersection  $x \sim$

$\alpha \log x$ .

The short-range part of the interaction is responsible for the initial linear light cone, which reasonably gives the  $\alpha$  independence in point (2). In contrast, the long-range part of the power law interaction contributes to the late time log light cone. The separation of short-range and long-range parts is not clear when  $\alpha < 3$ , so the linear light cone disappears, which implies the absence of intersection in point (3). This result indicates that a local perturbation first propagates linearly with time and then grows up exponentially with time. Similar linear followed by logarithmic light cone behavior has also been discussed in Ref. 30. Notice that we do not observe any power-law light cone regime here.

We further study the shape of  $\overline{h(x,t)}$ . We find that in the log light cone regime, we can collapse all the curves into a single curve with the scaling parameter as  $x/(v_B t)$  (Fig. 10(a) and Fig. 10(c)). We notice that  $\overline{h(x,t)}$  has a power decay  $\sim x^{-c}$  and an exponential dependence on time. This indicates that  $\overline{h(x,t)} \sim e^{\lambda t}/x^c$  when  $\overline{h(x,t)} \ll 1$ . In the linear light cone regime,  $\overline{h(x,t)}$  forms a stable traveling wave since we can collapse all the curves into a single curve by directly using  $x - v_B t$  as a scaling parameter. Around  $x = v_B t$ , the traveling wave takes a simple form  $\exp(\lambda(t - x/v_B))$ . We believe the physics here is very similar to Eq. (2.9), which describes the dynamics of  $\overline{h(x,t)}$  in systems with local interaction and has a stable traveling wave solution.

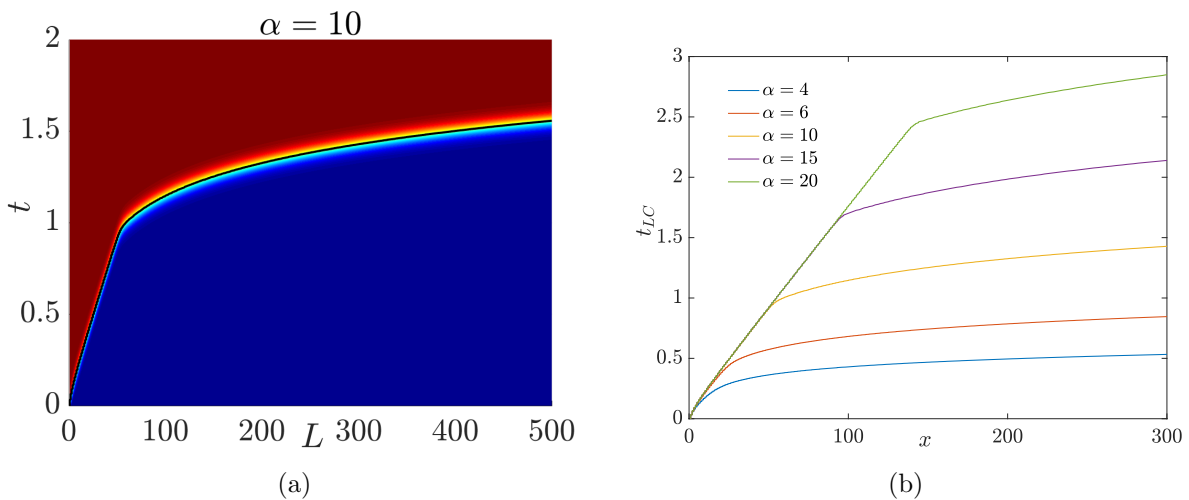


FIG. 9. (a) The boundary curve (light cone) switches from linear to logarithmic in the large  $N$  limit at  $\alpha = 10$ . (b) The transition from linear light cone to log light cone at various  $\alpha$ .

Based on the above analysis, we find that there are differences between  $N = 1$  and  $N = \infty$  cases. This large  $N$  solution can be understood as the mean field solution of the master

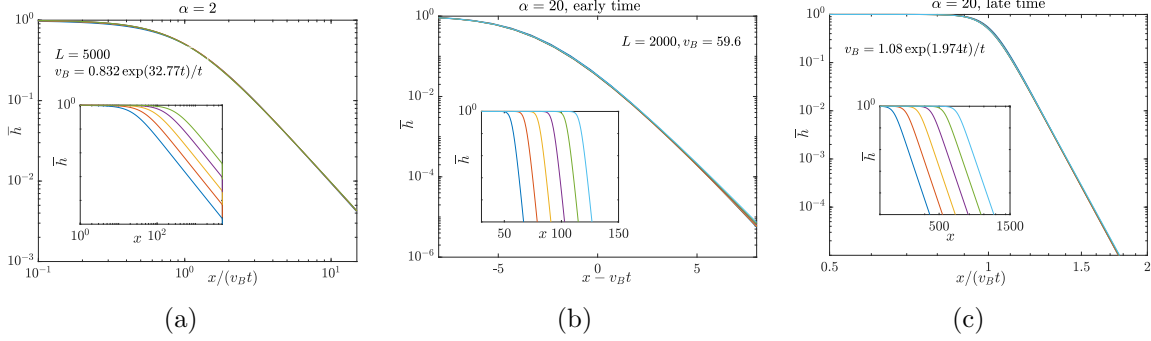


FIG. 10. Data collapse of  $\overline{h(x)}$  curves in the large  $N$  limit for various  $\alpha$ . The curves before collapsing are shown in the inset. (a) Scaling collapse on the log-log scale at  $\alpha = 2$ . The curves in the inset have  $t \in [0.1, 0.18]$  in steps 0.02. (b) Scaling collapse on the semi-log scale at early time in the linear light cone regime. The curves in the inset have  $t \in [1, 2]$  in steps 0.2. (c) Scaling collapse on the log-log scale at late time in the log light cone regime. The curves in the inset have  $t \in [2.75, 3.25]$  in steps 0.1.

equation, which ignores the height fluctuation over different samples. It only works at small  $\alpha$  and does not hold for large  $\alpha$  when fluctuation is strong.

As argued in Ref. 12, in the system with local interaction, the large  $N$  solution is unstable against the  $1/N$  corrections. In the long time limit, the  $1/N$  correction can be understood by a noise term that will lead to a diffusively broadening of the wavefront, which is essentially the same as the small  $N$  limit. We expect the same mechanism to work in the power law interaction systems. As long as  $N$  is finite, the large  $N$  solution is unstable. When  $\alpha$  is large, we will only observe the linear light cone rather than the two-segment light cones behavior. The scaling of OTOC will be described by the diffusive wavefront picture. A power law light cone which is found in  $N = 1$  case may also occur. A simple way to study these behaviors is to introduce noise term in Eq. (2.8), which we leave for future work.

## V. CONCLUSION AND OUTLOOK

In conclusion, we use OTOC to measure chaos propagation in one dimensional power law interaction systems in which each site has  $N$  qubits. In the  $N = 1$  limit, by using OTOC to define light cone, we find that (1) a log light cone regime when  $1 < \alpha < 2$ , (2) a power law light cone regime when  $2 < \alpha < 4$  and (3) an emergent linear light cone regime when  $\alpha > 4$ . We further compute the scaling function of OTOC and find that as  $\alpha$  is slightly larger than 4, the chaos dynamics is essentially the same as that for systems with short-range

interactions. Therefore it can be described by the diffusive wavefront picture, suggesting that the locality is fully recovered in the long-range power law interaction systems. In the power law light cone regime, we notice that it can be further divided into two subregimes according to the different scaling behavior of OTOC. We find that in one subregime with smaller  $\alpha$ ,  $C(t) \sim (t^b/x)^c$  if  $C(x, t) \ll 1$ , i.e, an algebraic dependence in both temporal and spatial directions. As we reduce to  $\alpha < 2$  in log light cone regime, the above scaling function is replaced by  $C(t, x) \sim \exp(\lambda t)/x^c$ . Finally, when  $\alpha < 1$ , there is no light cone and  $C(t, x)$  shows similar behavior as in the  $\alpha = 0$  limit.

We also compute the scaling function of OTOC in the large  $N$  limit and find that there is a transition from early time linear light cone to late time log light cone behavior at large  $\alpha$ . We also comment on the stability of this late time log light cone at finite  $N$  and argue that the large  $N$  solution might be unstable against  $1/N$  correction.

There are several directions for generalization. First of all, our analysis on both the small  $N$  and large  $N$  limits can be extended to finite  $N$  and therefore provides a complete physical picture for chaos dynamics in long-range power law interaction system. The simulation of the stochastic process can also be used to study higher dimensions, to check whether the light cone bounds implied from quantum information constraints can be saturated in this system. Another interesting direction is to investigate the entanglement growth for this non-local interaction, in particular entanglement velocity  $v_E$  as the growth rate as we vary  $\alpha$ . We expect to have better understandings on these interesting issues in the future.

## ACKNOWLEDGMENTS

We acknowledge useful discussion with Sarang Gopalakrishnan, Rajibul Islam, Austen Lamacraft, Andreas W.W. Ludwig, Marcos Rigol, Shinsei Ryu and Cenke Xu. We also thank the accommodation and interactive environment of the KITP program “The Dynamics of Quantum Information”. XC and TZ are supported by postdoctoral fellowships from the Gordon and Betty Moore Foundation, under the EPiQS initiative, Grant GBMF4304, at the Kavli Institute for Theoretical Physics. We acknowledge support from the Center for Scientific Computing from the CNSI, MRL: an NSF MRSEC (DMR-1720256) and NSF

- 
- <sup>1</sup> A. I. Larkin and Yu. N. Ovchinnikov. Quasiclassical Method in the Theory of Superconductivity. *Soviet Journal of Experimental and Theoretical Physics*, 28:1200, June 1969.
- <sup>2</sup> Patrick Hayden and John Preskill. Black holes as mirrors: quantum information in random subsystems. *Journal of High Energy Physics*, 2007(09):120, 2007.
- <sup>3</sup> Yasuhiro Sekino and L. Susskind. Fast scramblers. *Journal of High Energy Physics*, 2008(10):065, 2008.
- <sup>4</sup> A. Kitaev, 2015. Talks at KITP, April 7, 2015 and May 27, 2015.
- <sup>5</sup> D. A. Roberts, D. Stanford, and L. Susskind. Localized shocks. *Journal of High Energy Physics*, 3:51, March 2015. arXiv: 1409.8180.
- <sup>6</sup> Juan Maldacena and Douglas Stanford. Remarks on the sachdev-ye-kitaev model. *Phys. Rev. D*, 94:106002, Nov 2016.
- <sup>7</sup> Stephen H. Shenker and Douglas Stanford. Black holes and the butterfly effect. *Journal of High Energy Physics*, 2014(3):1–25, 2014.
- <sup>8</sup> Daniel A. Roberts and Douglas Stanford. Diagnosing chaos using four-point functions in two-dimensional conformal field theory. *Phys. Rev. Lett.*, 115:131603, Sep 2015.
- <sup>9</sup> Elliott H. Lieb and Derek W. Robinson. The finite group velocity of quantum spin systems. *Communications in Mathematical Physics*, 28(3):251–257, Sep 1972.
- <sup>10</sup> C. W. von Keyserlingk, Tibor Rakovszky, Frank Pollmann, and S. L. Sondhi. Operator hydrodynamics, otocs, and entanglement growth in systems without conservation laws. *Phys. Rev. X*, 8:021013, Apr 2018.
- <sup>11</sup> Adam Nahum, Sagar Vijay, and Jeongwan Haah. Operator spreading in random unitary circuits. *Phys. Rev. X*, 8:021014, Apr 2018.
- <sup>12</sup> S. Xu and B. Swingle. Accessing scrambling using matrix product operators. *ArXiv e-prints*, February 2018. arXiv: 1802.00801.
- <sup>13</sup> V. Khemani, D. A. Huse, and A. Nahum. Velocity-dependent Lyapunov exponents in many-body quantum, semi-classical, and classical chaos. *ArXiv e-prints*, March 2018. arXiv: 1803.05902.
- <sup>14</sup> Matthew B. Hastings and Tohru Koma. Spectral gap and exponential decay of correlations. *Communications in Mathematical Physics*, 265(3):781–804, Aug 2006.

- <sup>15</sup> Michael Foss-Feig, Zhe-Xuan Gong, Charles W. Clark, and Alexey V. Gorshkov. Nearly linear light cones in long-range interacting quantum systems. *Phys. Rev. Lett.*, 114:157201, Apr 2015.
- <sup>16</sup> Nima Lashkari, Douglas Stanford, Matthew Hastings, Tobias Osborne, and Patrick Hayden. Towards the fast scrambling conjecture. *Journal of High Energy Physics*, 2013(4):22, Apr 2013.
- <sup>17</sup> Tianci Zhou and Xiao Chen. Operator Dynamics in Brownian Quantum Circuit. *arXiv:1805.09307 [cond-mat, physics:hep-th]*, May 2018. arXiv: 1805.09307.
- <sup>18</sup> Shenglong Xu and Brian Swingle. Locality, Quantum Fluctuations, and Scrambling. *arXiv:1805.05376 [cond-mat, physics:hep-th, physics:quant-ph]*, May 2018. arXiv: 1805.05376.
- <sup>19</sup> D. J. Luitz and Y. Bar Lev. Emergent locality in systems with power-law interactions. *ArXiv e-prints*, May 2018. arXiv: 1805.06895.
- <sup>20</sup> Eyal Leviatan, Frank Pollmann, Jens H. Bardarson, and Ehud Altman. Quantum thermalization dynamics with Matrix-Product States. *arXiv:1702.08894 [cond-mat, physics:quant-ph]*, February 2017. arXiv: 1702.08894.
- <sup>21</sup> Nima Lashkari, Douglas Stanford, Matthew Hastings, Tobias Osborne, and Patrick Hayden. Towards the fast scrambling conjecture. *Journal of High Energy Physics*, 2013(4), April 2013. arXiv: 1111.6580.
- <sup>22</sup> Hrant Gharibyan, Masanori Hanada, Stephen H. Shenker, and Masaki Tezuka. Onset of random matrix behavior in scrambling systems. *Journal of High Energy Physics*, 2018(7):124, Jul 2018.
- <sup>23</sup> D. A. Roberts, D. Stanford, and A. Streicher. Operator growth in the SYK model. *ArXiv e-prints*, February 2018. arXiv: 1802.02633.
- <sup>24</sup> P. C. Hohenberg and B. I. Halperin. Theory of dynamic critical phenomena. *Rev. Mod. Phys.*, 49:435–479, Jul 1977.
- <sup>25</sup> R. A. FISHER. The wave of advance of advantageous genes. *Annals of Eugenics*, 7(4):355–369, 1937.
- <sup>26</sup> AN Kolmogorov, IG Petrovskii, and NS Piskunov. A study of the diffusion equation with increase in the amount of substance, and its application to a biological problem. *Selected Works of AN Kolmogorov I*, pages 248–270, 1937.
- <sup>27</sup> Mark J. Ablowitz and Anthony Zeppetella. Explicit solutions of fisher’s equation for a special wave speed. *Bulletin of Mathematical Biology*, 41(6):835–840, Nov 1979.
- <sup>28</sup> Xiao Chen and Tianci Zhou. Operator scrambling and quantum chaos. *arXiv:1804.08655 [cond-mat, physics:hep-th, physics:quant-ph]*, April 2018. arXiv: 1804.08655.

- <sup>29</sup> Xiao Chen, Tianci Zhou, and Cenke Xu. Measuring the distance between quantum many-body wave functions. *Journal of Statistical Mechanics: Theory and Experiment*, 2018(7):073101, 2018.
- <sup>30</sup> Zhe-Xuan Gong, Michael Foss-Feig, Spyridon Michalakis, and Alexey V. Gorshkov. Persistence of locality in systems with power-law interactions. *Phys. Rev. Lett.*, 113:030602, Jul 2014.